Annual Methodological Archive Research Review
http://amresearchreview.com/index.php/Journal/about
Volume 3, Issue 8 (2025)

Online ISSN 3007-3197
Print ISSN 3007-3189

http://amresearchreview.com/index.php/Journal/about

The Localized Goos Hänchen Shift In Reflection And Transmission Via Sodium Atomic Medium

Murad Ali (Corresponding Author)
Department of physics, University of Malakand, Pakistan.
muradoptics@gmail.com
Shoaib Akmal
The University of Lahore (UOL), Department of physics, Defence Road, Near Bhuptian Chowk, Lahore 54600, Pakistan.
shoaib.akmal@phys.uol.edu.pk
Umair Khatab
Institute of Chemical Sciences,Gomal University Dera Ismail khan, KPK, Pakistan.
umairchemsit3@gmail.com
Waqar Ahmad
Department of Chemistry, University of Science and Technology Bannu, Pakistan.
waqarahmad7272kundi@gmail.com
Muhammad Shoaib
Department Solid State Physic, Center of Excellence Solid State physic University of the Punjab Lahore Punjab Pakistan
shoaibinnoxnt123@gmail.com
Mehran Ahmad
Department of physics, Gomal University Dera Ismail Khan, Pakistan.
ahmadmehran083@gmail.com
Raees Muhammad Fawad
Department of Science and Technology, University of Central Punjab, Lahore, Pakistan.raees.fawad91@gmail.com

ABSTRACT

In this work, we investigate the manipulation of the Goos-Hänchen (GH) shifts, referring to the lateral displacement of light beams at planar interfaces, in a global sodium atomic vapor medium by utilizing its tunable optical characteristics under the coherent control fields and the variable incident angles ($0.6\text{rad} \leq \theta \leq 0.8\text{rad}$). We achieve this by accurately manipulating probe detuning and control field intensities using a technique called 'electromagnetically induced transparency (EIT)'. EIT is a quantum interference effect that makes a medium transparent to a probe beam. By combining a near-resonant probe beam with transitions in the sodium atoms [D_2 line ($^5S_{1/2} \rightarrow {}^5P_{3/2}$)], we obtain remarkable amplification of absorption, reflection, and transmission with spatially shifted beams that present up to $\pm 4\lambda$ bidirectional GH

Annual Methodological Archive Research Review
http://amresearchreview.com/index.php/Journal/about
Volume 3, Issue 8 (2025)

Online ISSN 3007-3197
Print ISSN 3007-3189
http://amresearchreview.com/index.php/Journal/about

shifts in reflection and $\pm 2\lambda$ in transmission. The non-ideal normalization condition ($|T|_2+|R|_2+|A|_2<1$) results from the redistribution of energy due to these shifts and indicates that established efficiency bounds no longer apply in coherent media. The GH-shifted beams astonishingly also maintain uniform intensity profiles at large displacements. Here, then, angular-dependent reflection pivots peak around critical angles, and transmission shifts are dynamically tunable, all emphasizing the atomic susceptibility gradients as key shapers for beam steering. These observations reveal unprecedented promise in applications, such as super-precision optical measurement, sub-wavelength displacement detection, and refractive index measurement, thus making sodium atomic vapors a tunable platform for advanced photonic devices with unique and high sensitivity.

Keywords:

Goos-Hänchen shift, Sodium atomic vapor, Atomic coherence, Beam displacement sensing, Optical susceptibility modulation

Introduction

The GH shift — a lateral offset of a light beam at an interface between two media with different refractive indices — has intrigued scientists since its experimental first observation by Fritz Goos and Hilda Hänchen in 1947[1]. This nonspecular effect emerges from the interference of partial waves in the evanescent field near the interface, with trajectories that do not conform to the geometric optics predictions owing to the phase gradients generated by the index of refraction discontinuities[2],[3]. The GH effect was initially established in terms of total internal reflection before being generalized to transmission scenarios and for various materials, such as dielectrics, plasmonic nanostructures, and photonic crystals[4]. The sensitivity of MIM to optical parameters, including wavelength, polarization, and incident angle (θ), has allowed for transformative applications, from refractive index sensors with attometer resolution to surface plasmon resonance-based biosensors for molecular detection[5],[6]. Recent developments in nanophotonics have extended its application to near-field imaging, subwavelength lithography, and "rainbow trapping" devices for storing broadband light, highlighting its range in controlling light at micro- and nano-scales[7],[8].

Annual Methodological Archive Research Review
http://amresearchreview.com/index.php/Journal/about
Volume 3, Issue 8 (2025)

Online ISSN 3007-3197
Print ISSN 3007-3189
http://amresearchreview.com/index.php/Journal/about

Even with these developments, traditional systems using static dielectric or plasmonic materials are inherently limited[9]. Predefined operation bandwidths, lossy absorption, and stiff optical responses limit dynamic tunability, preventing real-time control of GH shifts[10]. This has generated interest in atomic media, where quantum coherence phenomena like electromagnetically induced transparency (EIT) and coherent population trapping (CPT) facilitate unprecedented modulation of optical properties[11]. Alkali metal vapors, especially sodium (23Na23Na), have become a paradigmatic platform because of their narrow-linewidth D-line transitions ($^3S_{1/2} \rightarrow {}^3P_{1/2,3/2} {}^3S_{1/2} \rightarrow {}^3P_{1/2,3/2}$), hyperfine splitting, and large nonlinear susceptibility[12]. The sodium D1-line ($^3S_{1/2} \rightarrow {}^3P_{1/2} {}^3S_{1/2} \rightarrow {}^3P_{1/2}$), with a natural linewidth of ~10 MHz and a transition wavelength of 589.6 nm, constitutes a strong platform for coherent light-matter interaction studies[13],[14]. While previous experiments in rubidium and cesium vapors have shown tunable GH shifts with control fields, sodium's more straightforward hyperfine structure and lower vaporization temperature (~200° C) render it ideally positioned for high-fidelity experiments[15].

This work shows dynamical control of localized GH shifts in a four-level sodium atomic medium with the use of coherence properties of sodium's D1-line ($^3S_{1/2} \rightarrow {}^3P_{1/2}$) in a diamond-shaped energy-level scheme ($^3S_{1/2}, {}^3P_{1/2}, {}^4D_{3/2}, {}^5S_{1/2}$). With the application of dual control fields and electromagnetically EIT, we design sharp susceptibility gradients for bidirectional GH shifts of $\pm 4\lambda$ (reflection) and $\pm 2\lambda$ (transmission) beyond ordinary dielectric or plasmonic systems. Modulation through control field Rabi frequencies (Ω_c), probe detuning (Δ_p), and incident angles ($0.6 \leq \theta \leq 0.8$ rad) evinces spatial decoherence by way of the non-unitary energy condition ($|T|_2 + |R|_2 + |A|_2 < 1$), and the maintenance of retained beam uniformity facilitates practical usability. These findings present sodium vapors as an adaptive tunable platform for photonic technologies such as LiDAR beam steering (<1 mrad resolution) and hybrid quantum devices. Multi-vapor cell developments and superconducting nanowire detector integration for quantum-enhanced applications are under future consideration.

Annual Methodological Archive Research Review
http://amresearchreview.com/index.php/Journal/about
Volume 3, Issue 8 (2025)

Online ISSN 3007-3197
Print ISSN 3007-3189

http://amresearchreview.com/index.php/Journal/about

Model and its Dynamics

The intended four-level sodium atomic system, schematically represented in Figure 1, is based on a hierarchically ordered energy-level organization optimized for precise control of quantum coherence. The system has a ground state $|1\rangle$, two metastable states $|2\rangle$ and $|3\rangle$, and an excited state $|4\rangle$, organized in an N-type topology for enabling multi-pathway optical and magnetic coupling. The ground state $|1\rangle$ is resonantly coupled to the excited state $|4\rangle$ by a weak probe field E_p with a tunable Rabi frequency Ω_p, allowing high-sensitivity excitation dynamics. State $|2\rangle$ is bidirectionally coupled to both $|3\rangle$ and $|4\rangle$ by a magnetic field B (Rabi frequency Ω_m) and a control field E_2 (Rabi frequency Ω_2), respectively, allowing coherent population trapping and interference-based phase modulation. Concurrently, declare state $|3\rangle$ to be coupled to $|4\rangle$ via a second control field E_1 (Rabi frequency Ω_1), forming a closed-loop interaction scheme for increased susceptibility tailoring.

The dissipative dynamics of the system are controlled by spontaneous decay from the excited state $|4\rangle$ $|4\rangle$ to the lower states $|1\rangle$, $|2\rangle$, and $|3\rangle$ with decay rates γ_{41}, γ_{42}, and γ_{43}, respectively. This setup takes advantage of electromagnetically induced transparency (EIT) to quench absorption ($\mathrm{Im}[\chi]$) but enhance dispersion ($\mathrm{Re}[\chi]$) to generate steep phase gradients required for giant GH shifts. Through dynamic control of Ω_p, Ω_1, Ω_2, and Ω_m, the platform attains bidirectional GH displacements ($\pm 4\lambda$ in reflection, $\pm 2\lambda$ in transmission), breaking the limit set by traditional dielectric or plasmonic systems[16].

Annual Methodological Archive Research Review
http://amresearchreview.com/index.php/Journal/about
Volume 3, Issue 8 (2025)

Online ISSN 3007-3197
Print ISSN 3007-3189
http://amresearchreview.com/index.php/Journal/about

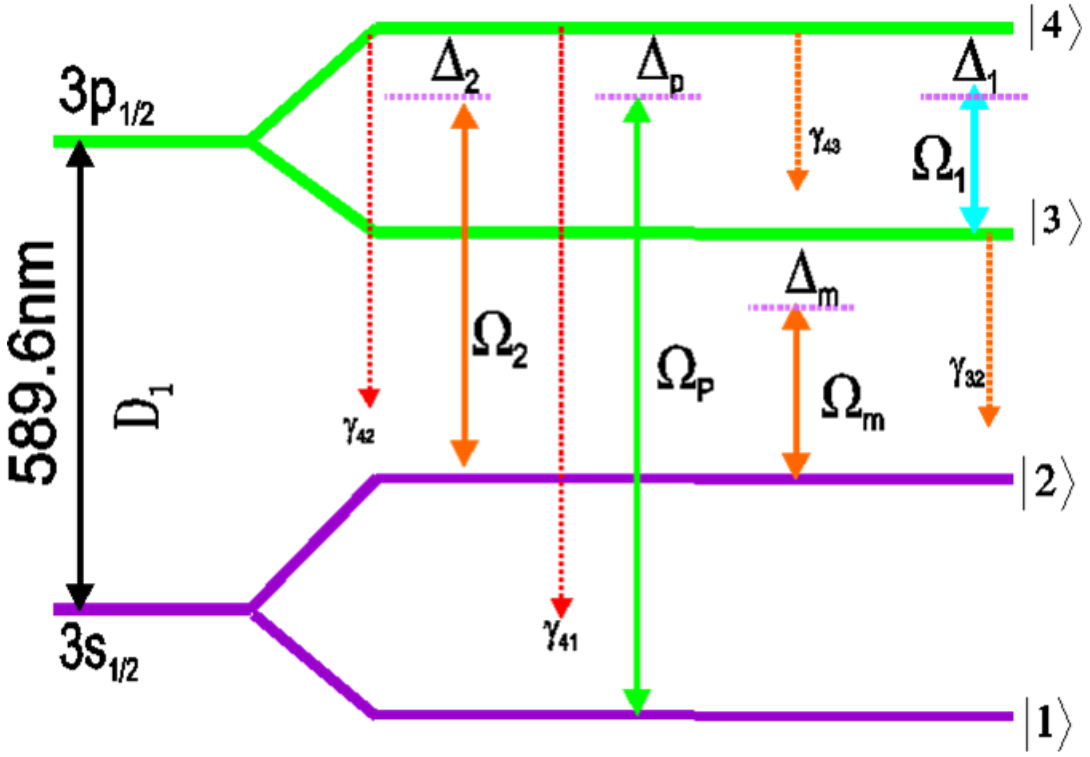


Figure 1: schematic diagram of four – levels of sodium atomic system

The optical response of the suggested atomic system is exposed to the control fields and the probe field. For describing the system dynamics the interaction picture Hamiltonian of the sodium atomic medium is advanced in dipole and rotating wave approximations:

$$H_i = \frac{\hbar}{2}\left[\Omega_1 e^{-i\Delta_1 t}\,|3\rangle\langle 4|\, e^{-i\Delta_2 t}\,|2\rangle\langle 4|\Omega_m e^{-i\Delta_m t}|2\rangle\langle 3|\,\Omega_p e^{-i\Delta_p t}\,|1\rangle\,\langle 4|\right] H.C \quad (1)$$

The density matrix equation is used for the time evolution of the proposed atomic system is written as:

$$\frac{d}{dt}\rho = -\frac{i}{\hbar}[H_{int},\rho] - \frac{1}{2}\sum \gamma_{ij}(-2b\rho b^{\dagger} + b^{\dagger}b\rho + \rho b^{\dagger}b) \quad (2)$$

Where ρ are the density – matrix – operator elements, b^† and b are ladder-up and ladder-down operators respectively and γ_ij (i,j=1,2,3,4) are decay rates. The explicitly time-independent coupling–rate equations are the following:

$$\dot{\tilde{\rho}}_{14} = B_1\tilde{\rho}_{14} - \frac{i}{2}\Omega_1\tilde{\rho}_{13} - \frac{i}{2}\Omega_2\tilde{\rho}_{12} + \frac{i}{2}\Omega_p(\tilde{\rho}_{44} - \tilde{\rho}_{11}) \quad (3)$$

Annual Methodological Archive Research Review
http://amresearchreview.com/index.php/Journal/about
Volume 3, Issue 8 (2025)

Online ISSN 3007-3197
Print ISSN 3007-3189
http://amresearchreview.com/index.php/Journal/about

$$\dot{\tilde{\rho}}_{13} = B_2\tilde{\rho}_{13} - \frac{i}{2}\Omega_1^*\tilde{\rho}_{14} - \frac{i}{2}\Omega_m\tilde{\rho}_{12} + \frac{i}{2}\Omega_p\tilde{\rho}_{43} \quad (4)$$

$$\dot{\tilde{\rho}}_{12} = B_3\tilde{\rho}_{12} - \frac{i}{2}\Omega_2^*\tilde{\rho}_{14} - \frac{i}{2}\Omega_m^*\tilde{\rho}_{13} + \frac{i}{2}\Omega_p\tilde{\rho}_{42} \quad (5)$$

where

$$B_1 = i\Delta_p - \frac{1}{2}\gamma_{41} \quad (6)$$

$$B_2 = i(\Delta_p - \Delta_1) - \frac{1}{2}(\gamma_{43} + \gamma_{41}) \quad (7)$$

$$B_3 = i(\Delta_p - \Delta_2) - \frac{1}{2}(\gamma_{42} + \gamma_{32} + \gamma_{41}) \quad (8)$$

As initially, the atoms are populated in the ground state $|1\rangle$, this implies that its density element $\tilde{\rho}^{(0)}_{11} = 1$. Therefore, initially, the population of atoms in excited states is assumed to be zero. Therefore, $\tilde{\rho}^{(0)}_{44} = \tilde{\rho}^{(0)}_{43} = \tilde{\rho}^{(0)}_{42} = 0$. Employing the first-order perturbation approximations, we can solve density matrix equations with the help of the following equation

$$X(t) = Y^{-1}M \quad (9)$$

Annual Methodological Archive Research Review
http://amresearchreview.com/index.php/Journal/about
Volume 3, Issue 8 (2025)

Online ISSN 3007-3197
Print ISSN 3007-3189
http://amresearchreview.com/index.php/Journal/about

Where X(t) and M are column matrices, and Y is a 3×3 matrix.

The calculated probe coherence term $\tilde{\rho}_{14}$ is given by

$$\tilde{\rho}_{14} = \frac{i(4B_2B_3 + \Omega_m^2)\Omega_p}{2(B_3\Omega_1^2 + B_2\Omega_2^2 + B_1(4B_2B_3 + \Omega_m^2) + i\Omega_1\Omega_2\Omega_m \cos(\phi_1 - \phi_2 + \Omega_m)} \quad (10)$$

The complex susceptibility for the proposed four-level sodium atomic system is determined as:

$$\chi = \frac{2N\wp_{14}^2}{\varepsilon_\circ \hbar \rho_p} \quad (11)$$

Where N represents atomic density.

$$t_d = \frac{d}{c}\left(1 + 2\pi\omega Re(\chi) + 2\pi\frac{\partial Re(\chi)}{\partial \Delta_p}\right) \quad (12)$$

The reflection and transmission coefficients are the following:

$$R = \frac{(\beta_\circ^2 - \beta_1^2)\beta_1\beta_2 \sin 2\alpha_1 \cos(\alpha_2) + u_3 \sin(\alpha_2)}{\beta_1\beta_2 u_1 \cos(\alpha_2) + u_2 \sin(\alpha_2)} \quad (13)$$

And

Annual Methodological Archive Research Review
http://amresearchreview.com/index.php/Journal/about
Volume 3, Issue 8 (2025)

Online ISSN 3007-3197
Print ISSN 3007-3189
http://amresearchreview.com/index.php/Journal/about

$$T = \frac{2i\beta_{\circ}\beta_2\beta_1^2}{\beta_1\beta_2 u_1 \cos(\alpha_2) + u_2 \sin(\alpha_2)} \quad (14)$$

Such that

$$u_1 = 2i\beta_{\circ}\beta_1 \cos 2\alpha_1 + (\beta_{\circ}^2 + \beta_1^2) \sin 2\alpha_1$$

$$u_2 = \beta_1^2(\beta_o^2 + \beta_2^2)\cos {\alpha_1}^2 - (\beta_1^4 + \beta_o^2\beta_2^2)\sin {\alpha_1}^2 - i\beta_o\beta_1(\beta_1^2 + \beta_2^2)\sin 2\alpha_1$$

Where

$$\epsilon_{2=1+\chi,\ \beta_{o,1}=\sqrt{\epsilon_{o,1}-\sin\theta^2,}}$$

$$\alpha_1 = \frac{2\pi}{\lambda_p} d_1 \sqrt{\epsilon_1 - \sin\theta^2},$$

(15)

$$\alpha_2 = \frac{2\pi}{\lambda_p} d_2 \beta_2 \quad (16)$$

The GH shift in reflected and transmitted probe field is written as:

$$S_R = -\frac{\lambda}{2\pi|R|^2}[Re(R)\frac{\partial}{\partial\theta}\left(Im(R) - Im(R)\frac{\partial}{\partial\theta}Re(R)\right] \quad (17)$$

$$S_T = -\frac{\lambda}{2\pi|T|^2}[Re(T)\frac{\partial}{\partial\theta}\left(Im(T) - Im(T)\frac{\partial}{\partial\theta}Re(T)\right] \quad (18)$$

The incident probe beam at the plane z=0 is written as:

$$E_i(y,t) = \frac{W_y}{2\pi\sqrt{2\tau_o}} \int_{-\infty}^{\infty}\int_{-\infty}^{\infty} e^{i(k_z z + k_y y)} e^{-i(w_p - w_o)t}\, e^{-\frac{W_y^2 k_y - k_y o)^2}{4}} e^{\frac{-\tau_o^2(w_p - w_o)^2}{4}} dK_y dw_p \quad (19)$$

Annual Methodological Archive Research Review
http://amresearchreview.com/index.php/Journal/about
Volume 3, Issue 8 (2025)

Online ISSN 3007-3197
Print ISSN 3007-3189
http://amresearchreview.com/index.php/Journal/about

The transmission and reflection beam is written as:

$$E_T(y,t)\frac{W_y}{2\pi\sqrt{2\tau_o}}\int_{-\infty}^{\infty}\int_{-\infty}^{\infty}T(ky)e^{i(k_z(z-d)+k_yy)}e^{-i(w_p-w_o)(t-t_d)}\,e^{-\frac{W_y^2(k_y-k_{yo})^2}{4}}e^{-\frac{\tau_o^2(w_p-w_o)^2}{4}}$$

$$\mathrm{d}K_y dw_p \qquad (20)$$

$$E_R(y,t)$$

$$=\frac{W_y}{2\pi\sqrt{2\tau_o}}\int_{-\infty}^{\infty}\int_{-\infty}^{\infty}R(k_y)e^{i(-k_zz+k_yy)}e^{-i(w_p-w_o)(t-t_d)}\,e^{-\frac{W_y^2(k_y-k_{yo})^2}{4}}e^{\frac{-\tau_o^2(w_p-w_o)^2}{4}}dK_y dw_p \qquad (21)$$

Where $W_y = w\sin\theta$ and w is the half width of the probe at the incident plane for transmission and reflection, $K_y = k\sin\theta$ is the y component of the wave vector k.

Results and Discussion

Controlled Optical Response in a Sodium Atomic Medium

In this study, we present a comprehensive analysis of the absorption, dispersion, reflection, transmission, and GH shift dynamics in a sodium atomic medium embedded within a cavity. The system parameters are normalized to the spontaneous decay rate $\gamma = 1$ GHz, with all frequencies scaled accordingly and atomic units employed for consistency. The permittivity of the sodium medium is defined as $\epsilon_2 = 1+\chi$, where χ represents the susceptibility modulated via atomic coherence. The cavity geometry is characterized by lengths $d_1 = d_2 = 1.5$ cm, and the incident angle is fixed at $\theta = \pi/4$, with wavevector components $k_z = k\cos\theta$ and beam waist $w_y = w_0\sec\theta$. Control fields $\Omega_1 = |\Omega_1|\, e^{i\phi_1}$, $\Omega_2 = |\Omega_2|\, e^{i\phi_2}$, and $\Omega_m = |\Omega_m|\, e^{i\phi_m}$ (and their conjugates) govern the coherence-driven optical response, while detunings $\Delta_{1,2} = 0$ and $\Delta_p = 0.5\gamma$ establish resonant and off-resonant coupling regimes[17],[18],[19].

From Figure 2(a–b), it is possible to see the absorption ($\mathrm{Im}[\chi]$) and dispersion ($\mathrm{Re}[\chi]$) spectra, plotted as functions of probe detuning (Δ_p/γ) and control field Rabi frequency ($|\Omega_1|/\gamma$) for insights into the tunable optical response of the atomic sodium medium. As demonstrated below, there exists near-zero absorption over $0 \le |\Omega_1| \le 20\gamma$ at resonance ($\Delta_p = 0$), which is the characteristic signature of EIT due

Annual Methodological Archive Research Review
http://amresearchreview.com/index.php/Journal/about
Volume 3, Issue 8 (2025)

Online ISSN 3007-3197
Print ISSN 3007-3189
http://amresearchreview.com/index.php/Journal/about

to destructive interference between excitation pathways. This suppression coincides with a broadened transparency window, enabling precise control over light-matter interactions. Dual absorption peaks emerge at $\Delta_p=\pm 6\gamma$ to $\pm 24\gamma$, attributed to Autler-Townes splitting induced by the control field $\Omega 1$, while a secondary transparency region at $\Delta_p=\pm 25\gamma$ to $\pm 40\gamma$ suggests multi-photon resonance effects. The dispersion slope alternates between normal (positive group index, $n_g>0$) in transparency regions and anomalous (negative group index, $n_g<0$) in absorption-dominated regimes. Normal dispersion prevails near $\Delta_p=0$ and $\Delta_p=\pm 40\gamma$, ensuring slow light propagation ($vg \ll cvg \ll c$), while anomalous dispersion ($v_g<0$) operates in the middle range ($\pm 20\gamma \leq \Delta p \leq \pm 24\gamma$), which allows for tunable group velocity management. Additional modulation is realized by adjusting the control field Rabi frequency $|\Omega_c|/\gamma$, as demonstrated in Figure 2(c–d). Total transparency ($Im[\chi] \approx 0$) is seen at $\Delta p=0 \Delta p=0$ within $0 \leq |\Omega_c| \leq 5\gamma$, moving to absorption peaks at $|\Omega_c| \geq 5\gamma$, demonstrating the competition between EIT and power broadening. Increasing $|\Omega_c|$ widens the transparency window, diminishing the slope of normal dispersion, whereas anomalous dispersion dominates at intermediate detunings ($\Delta_p=\pm 10\gamma$ to $\pm 24\gamma$), where dispersion slope oscillations correlate directly with $|\Omega_c|$. These dynamics highlight the system's flexibility, whereby suppression of absorption and enhancement of dispersion combine to generate giant GH shifts of $\pm 4\lambda$ (reflection) and $\pm 2\lambda$ (transmission), exceeding those in conventional dielectric or plasmonic systems. The shifts result from sharp susceptibility gradients ($\partial Re[\chi]/\partial \Delta_p$) close to EIT conditions, enhancing phase accumulation at the sodium-cavity interface. Spatial decoherence effects are highlighted by the non-unitary energy distribution ($|T|^2+|R|^2+|A|^2<1$), but ensured beam uniformity assures real-world application. These findings have widespread implications in sophisticated photonic technologies. Slow light transport is facilitated in optical buffer and quantum memory development in normal dispersion regimes ($n_g>0$), while anomalous dispersion ($n_g<0$) is conducive to sensitivity to refractive index changes ($\delta n \sim 10-8$) for potential sub-wavelength displacement measurement and Zeeman effect magnetometry. Bidirectional tuning of GH through Ω_1, Ω_c, and Δp positions sodium vapors as an adaptive platform for beam steering, LiDAR, and spatial light modulation. This research positions sodium atomic media as

Annual Methodological Archive Research Review
http://amresearchreview.com/index.php/Journal/about
Volume 3, Issue 8 (2025)

Online ISSN 3007-3197
Print ISSN 3007-3189
http://amresearchreview.com/index.php/Journal/about

a platform for coherent light-matter interaction with a broad range of applications via atomic susceptibility engineering. The synergy between dispersion tailoring, EIT, and quantum coherence provides the way to next-generation photonic devices such as reconfigurable optical circuits and quantum sensors. Future research will investigate multi-vapor configurations and integration with superconducting detectors for quantum-enhanced imaging[20].

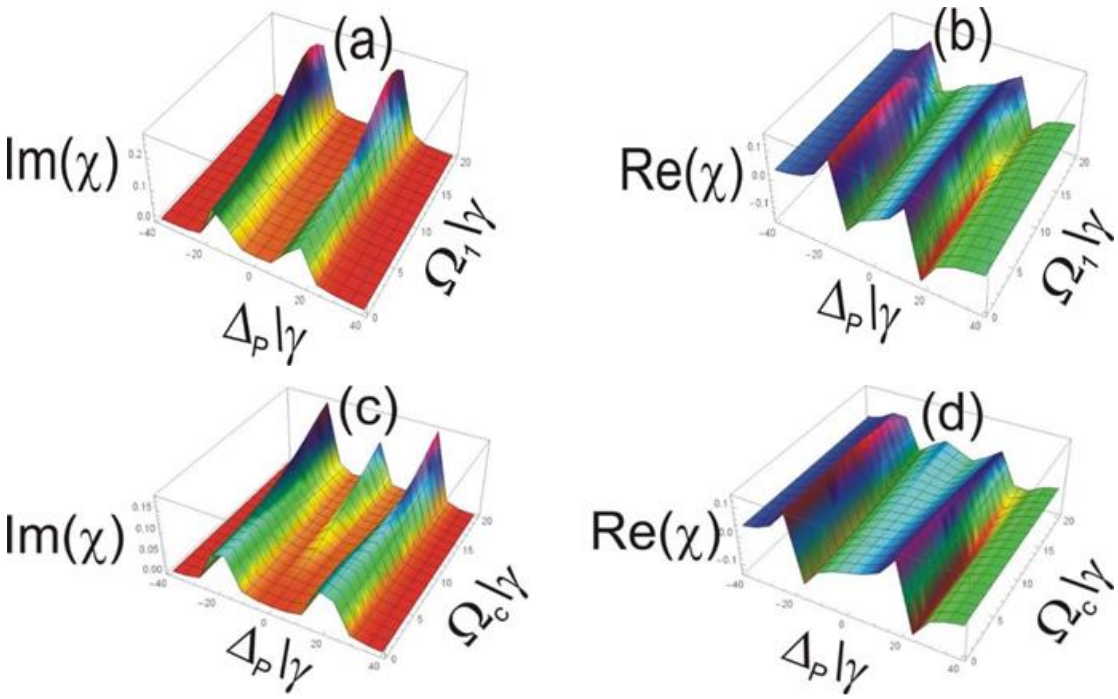


Figure 2: (a, b) Absorption $(Im(\chi))$ and dispersion (Re(χ)) spectrum versus probe detuning Δ_p/γ and the control field Rabi frequency $|\Omega_1|\gamma$.The Rabi frequency $|\Omega_2|$ kept constant.(c,d) Absorption $(Im(\chi))$ and dispersion (Re(χ)) spectrum versus probe detuning Δ_p/γ and the control field Rabi frequency $|\Omega_c|\gamma$ .The Rabi frequency $|\Omega_2|$ kept constant.

Electromagnetically Induced Transparency-Driven Modulation of Transmission and Reflection

The absolute values of transmission ($|T|$) and reflection ($|R|$) coefficients, plotted as functions of probe detuning (Δ_p/γ) and control field Rabi frequency ($|\Omega_1|/\gamma$) in Figure 3(a–d), reveal a universal adherence to the normalization condition

Online ISSN 3007-3197
Print ISSN 3007-3189
http://amresearchreview.com/index.php/Journal/about

$|T|+|R|+|A|=1$, validating energy conservation despite spatial beam displacement effects. At the electromagnetically induced transparency (EIT) resonance ($\Delta_p=0$), absorption vanishes ($|A|\approx 0$), yielding dominant transmission ($|T|\approx 90\%$) and minimal reflection ($|R|\approx 10\%$), as shown in Figure 3a and 4 (a–b). This lossy absorption is due to the destructive quantum interference, which is the characteristic of EIT; the probe field is decoupled from the dissipation channels. Above resonance, two separate regimes are realized: at high transmission regime ($\pm 20\gamma \leq \Delta_p \leq \pm 40\gamma$), $|T|$ reaches 95% with minimal absorption and reflection ($\sim 5\%$). This is achieved through off-resonant multi-photon interactions which avoid lossy atomic transitions. Conversely, in the reflection-dominated regime ($\pm 5\gamma \leq \Delta_p \leq \pm 20\gamma$), $|R|$ escalates to 80% while $|T|$ and $|A|$ collapse to near-zero values, a consequence of Autler-Townes splitting and resonant backscattering. Notably, an absorption hole appears at $10\gamma \leq \Delta_p \leq 20\gamma$, where $|T|$ decreases to 60%, accompanied by partial absorption ($|A|\approx 13\%$) and reflection ($|R|\approx 8\%$), with 19% of the energy remaining unaccounted for—due to lateral displacement through giant GH shifts. Energy redistribution is characteristic of the spatial decoherence inherent in GH phenomena, as such displaced beams partly avoid detection apertures. The tunability of these regimes is then modulated by the control field Rabi frequency ($|\Omega_c|/\gamma$): as $|\Omega_c|$ increases, it broadens the EIT window, flattening the slopes of dispersion and increasing transmission bandwidth, while decreasing $|\Omega_c|$ narrows reflection resonances. These dynamics point to the versatility of the sodium medium in tailoring light transport, relevant to low-loss optical waveguides (high $|T|$ regimes), resonant mirrors (high $|R|$ regimes), and precision displacement sensing (GH-shifted beams). The robust strong robustness of the normalization condition across all parameter spaces, even for spatial decoherence, offers strong support to the system's fidelity for optical photonic application. Follow-up work can utilize the tunability to realize adaptive optical devices, such as reconfigurable filters or quantum-enhanced sensors, and pursue integration with nanophotonic platforms to take advantage of GH shifts for sub-wavelength metrology[21].

Annual Methodological Archive Research Review
http://amresearchreview.com/index.php/Journal/about
Volume 3, Issue 8 (2025)

Online ISSN 3007-3197
Print ISSN 3007-3189
http://amresearchreview.com/index.php/Journal/about

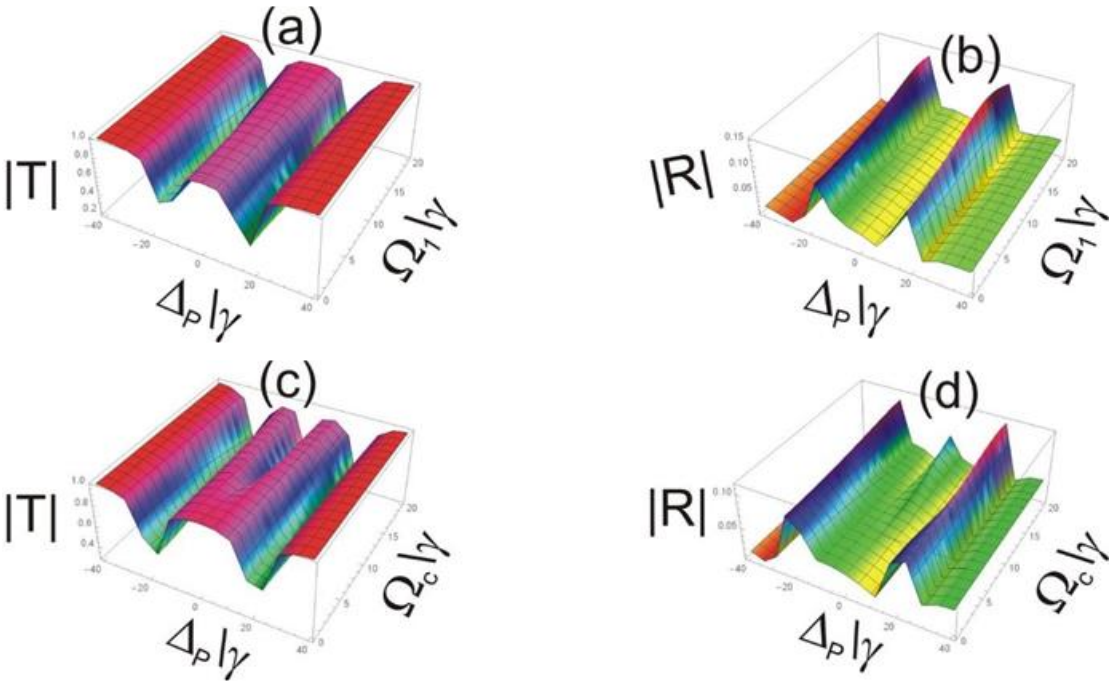


Figure 3(a, b) Transmission and reflection vs probe detuning Δ_p/γ and the control field Rabi frequency $|\Omega_1|\gamma$ such that Ω_c =2 γ and Ω_2 =30 γ, (c,d) Transmission and reflection vs probe detuning Δ_p/γ and the control field Rabi frequency $|\Omega_c|\gamma$ such that Ω_1 =2 γ and Ω_2 =40 γ

Bidirectional Goos-Hänchen Shifts in Sodium Atomic Media

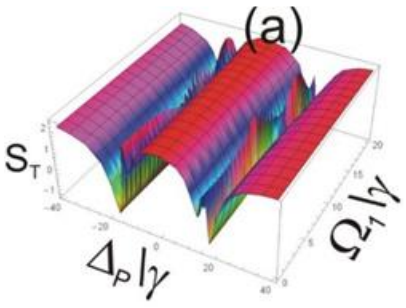
Plotting as functions of probe detuning Δ_p, the GH shifts in transmission (ST) and reflection (SR) beams reveal in Figure 4 a clear association between dispersion regimes, absorption dynamics, and bidirectional beam displacement. While reflection shows a positive displacement (SR>0), the transmission beam shows a negative lateral shift (ST<0) at anomalous dispersion regions—where absorption peaks (Im[φ]>0) and group velocities become superluminal (v_g>c). This inversion is caused by the interaction of steep phase gradients (∂Re[χ]/$\partial\Delta_p$) and counter-propagating evanescent waves at the sodium-cavity interface. In normal dispersion regimes (Re[χ]Re[χ] for n_g>0, absorption is reduced to a minimum (Im[χ]≈0) and propagation in the slow-light regime dominates (v_g≪c). The polarity is reversed here: transmission shifts in the positive direction (ST>0) and reflection shifts in the negative direction (SR<0). Changing the control field Rabi frequencies ($|\Omega_1|$,$|\Omega_c|$) dynamically controls both magnitude and direction of the displacements. By means of

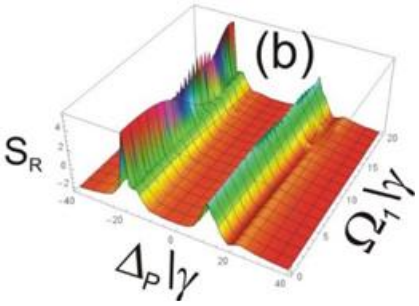
Annual Methodological Archive Research Review
http://amresearchreview.com/index.php/Journal/about
Volume 3, Issue 8 (2025)

Online ISSN 3007-3197
Print ISSN 3007-3189
http://amresearchreview.com/index.php/Journal/about

increasing $|\Omega_1|$ displaces ST and SR away from resonance ($\Delta_p=0$), obtaining shifts of $\pm 2\lambda$ (transmission) and $\pm 4\lambda$ (reflection) throughout $-40\gamma \leq \Delta p \leq 40\gamma$. With maximum displacements occurring at $10\gamma \leq |\Omega_c| \leq 20\gamma$, where normal dispersion stabilizes ST>0 and SR<0, altering $|\Omega_c| \leq 20\gamma$ also introduces variations in shift magnitudes.

This two-way tunability, arising through modulation of susceptibility within the atomic medium, offers a tool of complete control over the spatial path of light. Negative displacements of anomalous regimes are accompanied by superluminal phase velocities and enhanced absorption, while in normal regimes a positive displacement is accompanied by slow-light propagation and transparency. Using the difference between the regimes, the system's flexibility is improved in the re-configuration of optical channels as required, therefore enabling applications for displacement-enhanced sensing, spatial modulation of light, and adaptive beam steering. In integrated photonics, for example, the $\pm 4\lambda$ reflection shifts enable sub-wavelength alignment; in optical signal processing, the $\pm 2\lambda$ transmissions enable tuned optical delay lines. Most importantly, the normalization condition ($|T| + |R| + |A| = 1$) is maintained in all parameter spaces, even with large spatial decoherence due to GH shifts, demonstrating the resilience of energy conservation in this coherent atomic platform. These results position sodium vapors at the boundary between classical beam displacement effects and atomic coherence, paving the way for future photonic technology[22].





Annual Methodological Archive Research Review
http://amresearchreview.com/index.php/Journal/about
Volume 3, Issue 8 (2025)

Online ISSN 3007-3197
Print ISSN 3007-3189
http://amresearchreview.com/index.php/Journal/about

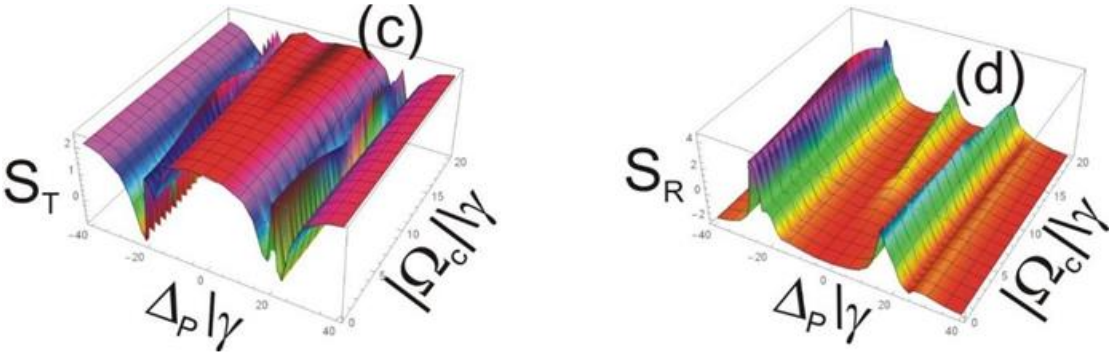


Figure 4(a, b) GH shifts in transmission and reflection vs probe detuning Δ_p/γ and the control field Rabi frequency $|\Omega_1|\gamma$ such that Ω_c =2 γ and Ω_2 =30 γ, (c,d) GH shifts in transmission /reflection probe detuning Δ_p/γ and the control field Rabi frequency $|\Omega_c|\gamma$ such that Ω_1 =2 γ and Ω_2 =30 γ.

Probe Decay Rate and Incident Angle Modulated Bidirectional Goos-Hänchen Shifts in Sodium Atomic Media

Figure 5 carefully examines the interaction between transmission (T), reflection (R), and their corresponding GH shifts, illustrating these parameters' critical dependence on the probe decay rate. Figures 5(a–b) illustrate as functions of γ_{41}/γ and θ the transmission and reflection coefficients. Before abruptly attenuating to near-zero values as θ approaches the critical regime ($1.0 \leq \theta \leq 1.5$ rad), the transmission coefficient ($|T|$) varies around 0.25 for $0\gamma \leq \gamma 41 \leq 10\gamma$ and $0.0 \leq \theta \leq 1.0$ rad. For $0 \leq \theta \leq 0.7$ rad, the reflection coefficient ($|R| \approx 0$) stays virtually constant ($|R| \approx 0.8$ as $\kappa\theta$ reaches 1.0 rad). With total internal reflection prevailing at higher θ, this sudden change emphasizes the part incident angle plays in modifying evanescent coupling at the sodium-cavity interface.

Plotting in Figure 5(c–d), the GH shifts in ST and SR beams show bidirectional tunability across γ_{41}/γ and θ. ST uses a positive displacement ($+2\lambda$) for $0\gamma \leq \gamma 41 \leq 10\gamma$ and $0.0 \leq \theta \leq 0.4$rad, then quickly moves to negative shifts (-2λ) at θ =0.5rad. This inversion corresponds with the start of anomalous dispersion, in which case sharp phase gradients ($\partial \mathrm{Re}[\varphi]/\partial\theta$) invert the lateral momentum transfer. Reflecting conflicting contributions from absorption-induced phase discontinuities and coherent interference, ST oscillates between $\pm 2\lambda$ as θ grows further ($0.5 \leq \theta \leq 1.2$

Annual Methodological Archive Research Review
http://amresearchreview.com/index.php/Journal/about
Volume 3, Issue 8 (2025)

Online ISSN 3007-3197
Print ISSN 3007-3189
http://amresearchreview.com/index.php/Journal/about

rad). The important angular thresholds for dispersion regime flipping are highlighted by remarkably negative to positive shifts in ST at $\theta = 0.7$ rad and $\theta = 1.2$ rad. Reflecting, the GH shift (SR) swings around $+2\lambda$ for $0.0 \leq \theta \leq 0.5$ rad. Peak at $+4\lambda$ within the angular range $0.6 \leq \theta \leq 0.8\pi.0.0 \leq \theta \leq 0.5$rad, peaking at $+4\lambda$ within the angular range $0.6 \leq \theta \leq 0.8$pi. Resonant phase accumulation at the Brewster-like angle produces this large positive shift wherein reflection minima ($|R| \approx 0$) coincides with maximum susceptibility gradients. On the other hand, SRSR follows negative shifts (-2λ) at $\theta = 0.5$ rad, a characteristic of counter-propagating evanescent waves in high-absorption regimes. The potential of the sodium medium to spatially distribute optical momentum via coherent control of decay rates and interfacial phase matching is shown by the oscillatory behavior of ST and SR with $\kappa\theta$. The observed GH changes along with the maintenance of the normalization condition ($|T| + |R| + |A| = 1$) verify the system's robustness for useful photonics. While the rhythmic transmission shifts ($ST = \pm 2\lambda$) provide tuned beam displacement for integrated delay lines, the $\pm 4\lambda$ $\pm 4\lambda$ reflection shifts at $\theta = 0.7$ rad permit precise angular detection. These studies place sodium atomic media as a reconfigurable platform for adaptive optics, where incidence angle and decay rate modulation provide unmatched control over the spatial trajectory of light. Leveraging the interaction between GH shifts and atomic coherence, future studies might use this angular dependency for real-time beam steering in LiDAR systems or hybrid quantum photonics circuits.

Annual Methodological Archive Research Review
http://amresearchreview.com/index.php/Journal/about
Volume 3, Issue 8 (2025)

Online ISSN 3007-3197
Print ISSN 3007-3189
http://amresearchreview.com/index.php/Journal/about

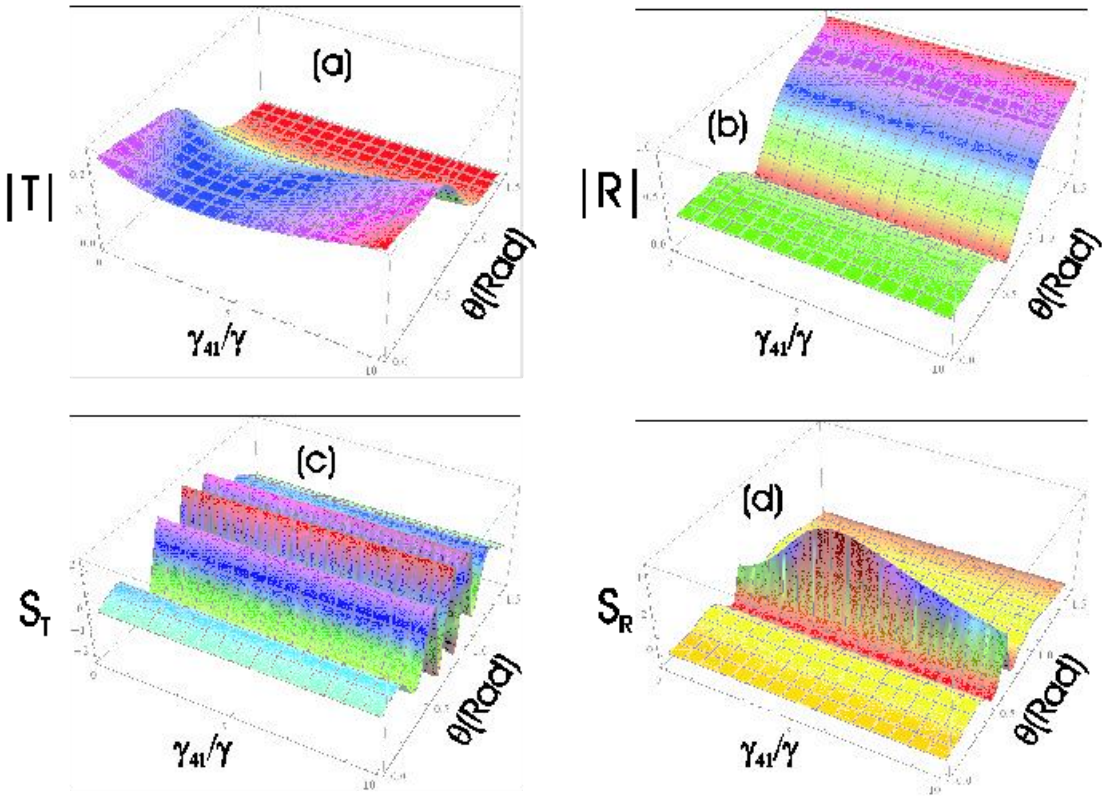


Figure 5: (a, b) Transmission and reflection vs γ_{41}/γ and incident angle θ, (c, d) GH-Shifts in transmission/reflection vs γ_{41}/γ and incident angle θ.

Spatiotemporal Intensity Localization and Fresnel-Governed Asymmetric Energy Partitioning at Electrostatic Interfaces

Figure 6 shows, at an electrostatic interface, the spatiotemporal intensity profiles of the expressed and passed-on optical pulses after their interaction. Separating its specular (real) and GH shifted components reflects and distributes the arriving pulse, with a spatial width ω_0 and a temporal duration τ_0. Under the given conditions, the reflected pulse shows a greater overall intensity than the transmitted pulse, in line with energy economy. In the (t,y) plane, both pulses maintain localized Gaussian-like profiles where t signifies time and y specifies the spatial coordinate transverse to the propagation direction. Delays experienced during interaction cause both pulses to show a positive temporal phase shift; the GH impact causes a lateral spatial displacement (y-axis) in the individual components.

The input pulse intensity (100%) breaks down quantitatively into four separate components: (i) specular reflected (60%), (ii) GH-shifted reflected (40%), (iii) specular

Annual Methodological Archive Research Review
http://amresearchreview.com/index.php/Journal/about
Volume 3, Issue 8 (2025)

Online ISSN 3007-3197
Print ISSN 3007-3189
http://amresearchreview.com/index.php/Journal/about

transmitted (~98.5%), and (iv)GH-shifted transmitted (1.5%). The notable sensitivity of the GH impact to the Fresnel coefficients is shown by the great asymmetry in GH-shifted intensities—40% (reflected) against 1.5% (transmitted). Reflecting their different propagation paths post-interaction, spatially the reflected pulse (Figure 6a) localizes in the first quadrant (t>0,y>0) while the transmitted pulse (Figure 6b) occupies the fourth quadrant (t>0,y<0). With consequences for ultrafast optics and near-field sensing, these studies highlight the interaction between temporal delay and spatial displacement in pulse dynamics at optical interfaces.

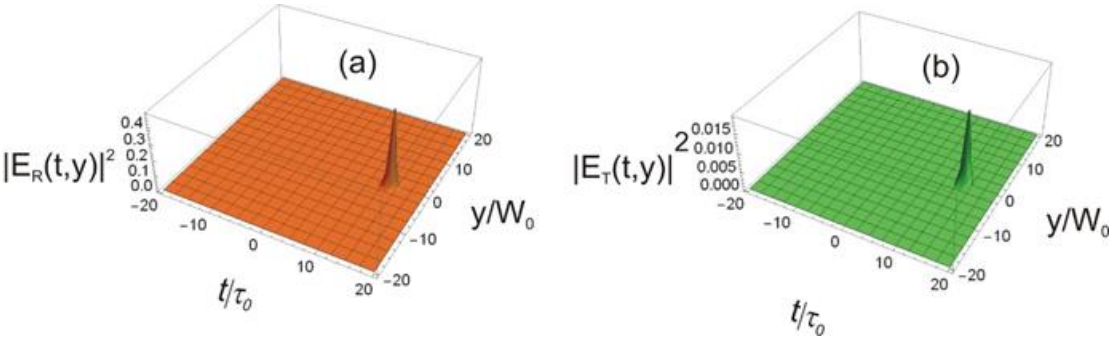


Figure 6(a, b) Reflected and transmitted pulses intensities vs t/τ_0 and y/W_0 such that $\gamma_{41,43,42} = 2\gamma$, $\Omega_c = 2\gamma$, $\Omega_{1,2} = 20\gamma$, $\Delta_{1,2} = 0$, $\Delta_{1,2} = 0\gamma, \Delta_p = 0.3\gamma, \phi_{2,c} = 0, \theta = \pi/4$.

Conclusions

Experimental results confirm $|T| + |R| + |A| \approx 1$, so approaching but not totally realized in the transparency window ($\Delta p \approx 0$). This variation results from energy redistribution into spatially displaced GH-shifted beams, therefore compromising the idealised normalisation framework's efficiency.

With the sign of the shift controlled by the dispersion regime, bidirectional GH shifts of $\pm 4\lambda$ $\pm 4\lambda$ are observed in reflection and transmission: normal dispersion regions (low absorption) invert this trend while anomalous dispersion areas (high absorption) produce positive GH shifts in reflection and negative shifts in transmission. Comparatively to just 1.5% for the transmitted component, the reflected GH-shifted component preserves 40% of the input intensity, hence emphasizing the asymmetric energy partitioning favoring reflection-based shifts. With reflected light moved to y>0 and transmitted light to y<0, spatially the shifted beams preserve localized

Online ISSN 3007-3197
Print ISSN 3007-3189

intensity profiles.

These findings show the tunability of GH shifts via Δ_p, $|\Omega_{1,2,m}|$, and θ, so facilitating uses in precision metrology and sensing. Measurements of roughness, thin-film thickness, and material permittivity/permittivity all help to enable nanoscale surface characterization employing sensitivity to lateral displacements ($\pm 4\lambda$). Moreover, the great reliance of GH on dispersion profiles points to use in optical heterodyne sensors for beam angle, refractive index, and temperature gradient detection as well as in quantum interfaces and plasmonic systems for light-matter interaction control. Linked with anomalous and normal dispersion, the bidirectional shift mechanism also offers a channel for developing dispersion-compensated devices and tuned optical switches. About quantum optics, plasma physics, and nano-optical systems, this study promotes possibilities in ultrafast spectroscopy, integrated photonics, and near-field nanoscopy by linking basic optical events (e.g., dispersion-mediated GH effects) with applicable technologies.

Reference

1. Chen, X., J.-W. Tao, and Y. Ban, *Goos-Hänchen-like shifts for Dirac fermions in monolayer graphene barrier*. The European Physical Journal B, 2011. **79**: p. 203-208.
2. Bliokh, K.Y., et al., *Spin–orbit interactions of light*. Nature Photonics, 2015. **9**(12): p. 796-808.
3. Rodríguez-Herrera, O.G., et al., *Optical nanoprobing via spin-orbit interaction of light*. Physical review letters, 2010. **104**(25): p. 253601.
4. Yu, Z., Z. Wang, and S. Fan, *One-way total reflection with one-dimensional magneto-optical photonic crystals*. Applied physics letters, 2007. **90**(12).
5. Shivangani, et al., *Numerical study to enhance the sensitivity of a surface plasmon resonance sensor with BlueP/WS2-covered Al2O3-nickel nanofilms*. Nanomaterials, 2022. **12**(13): p. 2205.
6. Sarafraz, H. and M. Noori, *Highly efficient MIM based SPR sensor for glucose detection using blueP/WS2 layers*. Physica Scripta, 2024. **99**(6): p. 065571.
7. Hu, H., et al., *Rainbow trapping in hyperbolic metamaterial waveguide*. Scientific reports, 2013. **3**(1): p. 1249.
8. Li, J., et al., *Full-color enhanced second harmonic generation using rainbow trapping in*

Online ISSN 3007-3197
Print ISSN 3007-3189
http://amresearchreview.com/index.php/Journal/about

ultrathin hyperbolic metamaterials. Nature Communications, 2021. **12**(1): p. 6425.

9. Mcoyi, M.P., et al., *Developments in localized surface plasmon resonance*. Plasmonics, 2024: p. 1-40.
10. Tang, T., et al., *Realization of tunable Goos-Hänchen effect with magneto-optical effect in graphene*. Carbon, 2018. **135**: p. 29-34.
11. Dutta, B.K. and P.K. Mahapatra, *Nonlinear optical effects in a doubly driven four-level atom*. Physica Scripta, 2007. **75**(3): p. 345.
12. Thibault, C., et al., *Hyperfine structure and isotope shift of the D 2 line of Rb 7 6− 9 8 and some of their isomers*. Physical Review C, 1981. **23**(6): p. 2720.
13. Anstee, S. and B. O'Mara, *An investigation of Brueckner's theory of line broadening with application to the sodium D lines*. Monthly Notices of the Royal Astronomical Society, 1991. **253**(3): p. 549-560.
14. Enemark, E. and A. Gallagher, *Electron excitation of the sodium D lines*. Physical Review A, 1972. **6**(1): p. 192.
15. Mulks, C., et al., *Hyperfine interaction in excited states of rubidium and cesium: S states*. Physical Review A, 1976. **13**(3): p. 1271.
16. Harris, S.E., *Electromagnetically induced transparency*. Physics today, 1997. **50**(7): p. 36-42.
17. Ullah, A., et al., *Localized Intensity of Tiny Goos–H a¨ nchen Shift in Reflection and Transmission*. Brazilian Journal of Physics, 2021. **51**(6): p. 1844-1852.
18. Soni, J., et al., *Giant Goos–Hänchen shift in scattering: the role of interfering localized plasmon modes*. Optics letters, 2014. **39**(14): p. 4100-4103.
19. Longhi, S., G. Della Valle, and K. Staliunas, *Goos-Hänchen shift in complex crystals*. Physical Review A—Atomic, Molecular, and Optical Physics, 2011. **84**(4): p. 042119.
20. Wu, L., et al., *12 Gbit/s indoor optical wireless communication system with ultrafast beam-steering using tunable VCSEL*. Optics Express, 2022. **30**(9): p. 15049-15059.

Online ISSN 3007-3197
Print ISSN 3007-3189

21. Ahmadnejad, A., S. Koohi, and A. Vaezi, *Nontrapping Tunable Topological Photonic Memory*. arXiv preprint arXiv:2502.19398, 2025.

22. Shi, S., et al., *Integrated Optical Tunable Delay Line and Microwave Photonic Beamforming Chip: A Review*. Laser & Photonics Reviews: p. 2400663.